Association of MRI indices of glymphatic system with amyloid β deposition and cognition in mild cognitive impairment and Alzheimer's disease

Koji Kamagata,[1,†] Christina Andica,[1,†] Kaito Takabayashi,[1] Yuya Saito,[1] Toshiaki Taoka,[2] Hayato Nozaki,[1] Junko Kikuta,[1] Shohei Fujita,[1] Akifumi Hagiwara,[1] Kouhei Kamiya,[3] Akihiko Wada,[1] Toshiaki Akashi,[1] Katsuhiro Sano,[1] Mitsuo Nishizawa[1], eMasaaki Hori,[3] Shinji Naganawa[2] and Shigeki Aoki[1], for the Alzheimer's Disease Neuroimaging Initiative*

SUPPLEMENTARY MATERIALS

eMethod 1

ADNI (https://adni.loni.usc.edu) was launched in 2003 as a public–private partnership led by principal investigator Michael W. Weiner, MD, of the San Francisco Veterans Affairs Medical Center and University of California, San Francisco (CA, USA). The primary goal of the ADNI has been to test whether serial MRI, PET, other biological markers, and clinical and neuropsychological assessments can be combined to measure the progression of MCI and early AD. A more detailed and up-to-date description of the ADNI is available at https://www.adni-info.org. This study only included patients for whom complete diffusion-weighted (DW), T1-weighted (T1w), and fluid-attenuated inversion recovery (FLAIR) imaging data were available. Previous studies have reported high intervendor variability in diffusion metrics and T_1 relaxation time[1, 2]. Therefore, we only selected participants for whom data were acquired using a GE scanner.

eMethod 2

The following neuropsychological tests were used in the present study: Mini-Mental State Examination, a brief questionnaire that measures global cognitive impairment[3]; Montreal Cognitive Assessment, a screening instrument for MCI and mild Alzheimer's disease[4]; Functional Activities Questionnaire, a questionnaire that rates patients' ability to independently complete activities of daily living;[5] Clinical Dementia Rating Scale Sum of Boxes, a test used to classify patients' cognitive status in six domains of cognitive and functional performance, namely, memory, orientation, judgment and problem solving, personal care, home and hobbies, and community affairs[6]; Rey Auditory Verbal Learning Test, a widely used test that evaluates anterograde verbal episodic memory in patients aged ≥16 years; Alzheimer's Disease Assessment Scale (ADAS),[7] including ADAS-11 (11 tasks assessing the memory, language, and praxis domains), ADAS-13 (13 tasks with additional tests of delayed word recall and a number cancellation or maze tasks), and ADAS-Q4 subscale (4 tasks assessing word recognition); logical memory total delayed recall, a measure of episodic memory[8]; and time to complete part B of the Trail Making Test, a measure of cognitive flexibility.[9]

eMethod 3

The modified Hachinski ischemic score was used as a tool to differentiate the types of dementia (primary degenerative, vascular or multi-infarct, or mixed type) in patients with MCI and Alzheimer's disease.[10] The CSF levels of Aβ42, phosphorylated tau, and total tau were also obtained from the ADNI-2 database. Additionally, data on PET SUVRs of [^{18}F] florbetapir (AV45), which is a marker of amyloid deposit, and [^{18}F]

fluorodeoxyglucose (FDG), which is a marker of glucose metabolism, were obtained from the ADNI-2 database. AV45-PET and FDG-PET SUVRs for each participant were calculated at the ADNI core laboratories following a standardized pipeline (https://adni.loni.usc.edu/methods/pet-analysis/).

eMethod 4

Imaging data were acquired using either a 3-T GE Signa HDx or Discovery MR750 scanner with two software versions, namely 15 m4 (https://adni.loni.usc.edu/wp-content/uploads/2010/05/ADNI_GO_GE_3T_15 m4_8chc.pdf) and 20.1 ib1 (https://adni.loni.usc.edu/wp-content/uploads/2010/05/ADNI_GO_GE_3T_201ib1_8ch b.pdf).

Diffusion-weighted (DW) imaging was performed with echo planar imaging sequence using the following parameters: b = 1000 s/mm2; 41 isotropic gradient directions; five non-DW (b0) volumes; echo time = 61.80–83.10 ms; repetition time = 9,500–14,200 ms; matrix size = 256 × 256; field of view = 350 × 350; and slice thickness = 2.7 mm. T1-weighted (T1w) imaging was performed with a spoiled gradient echo sequence using the following parameters: echo time = 2.83–3.17 ms; repetition time = 6.96–7.67 ms; matrix size = 256 × 256; field of view = 260 × 260 or 270 × 270; and slice thickness = 1.2 mm. Finally, fluid-attenuated inversion recovery (FLAIR) imaging was obtained with the following parameters: echo time = 147.90–153.90 ms; repetition time = 11,000 ms; inversion time = 2250 ms; matrix size = 256 × 256; field of view = 220 × 220; and slice thickness = 5 mm. More imaging details can be found at https://adni.loni.usc.edu/methods/documents/mri-protocols/.

eMethod 5

All T1w images were preprocessed, including subject motion correction, denoising, nonuniform intensity normalization, and skull stripping, using FreeSurfer 7.1.1 (https://surfer.nmr.mgh.harvard.edu). FLAIR images were then registered to the preprocessed T1w space using the FMRIB Linear Image Registration Tool of the FMRIB Software Library 6.0.3 (FSL; Oxford Centre for Functional MRI of the Brain, Oxford, UK; https://www.fmrib.ox.ac.uk/fsl) using trilinear interpolation and six degrees of freedom. This process resulted in a FLAIR-to-T1w image transformation matrix. The preprocessed T1w images were also used for the segmentation of cerebral WM, BG, and Hipp, which are known to be affected in Alzheimer's disease, using FreeSurfer. WM, BG, and Hipp masks were implemented in the calculation of the PVS volume and fractional volume of FW.

All DW images were assessed for severe artifacts, such as gross geometric distortion, signal dropout, and bulk motion, in the axial, sagittal, and coronal views. The EDDY tool, a part of FSL, was used to correct eddy current-induced distortions and subject movements in the DW data.[11] The DW images were then registered to the preprocessed T1w space with the epi_reg tool, a part of FSL, and the DW-to-T1w image transformation matrix was constructed. We also obtained the inverse transformation matrix (T1w-to-DW). The DTIFIT tool, a part of FSL, was used to generate the fractional anisotropy (FA) and mean diffusivity maps of all participants based on the ordinary least squares method.[12] FSL was also used to obtain diffusivity maps in the directions of the *x*-axis (right–left; D_{xx}), *y*-axis (anterior–posterior; D_{yy}), and *z*-axis (inferior–superior; D_{zz}).

eMethod 6

In computing the PVS map, the Frangi filter,[13] which estimates a vesselness measure for each voxel eigenvector of the Hessian matrix of the image, was applied to preprocessed T1w images using scikit-image library 0.19.1 (https://scikit-image.org/).[14] The default parameters ($\alpha = 0.5, \beta = 0.5$) of the Frangi filter were used.[13] However, parameter c was set to half the value of the maximum Hessian norm according to a previous study.[15] The Frangi filter estimated vesselness measures as different scales from 0.1 to 5 voxels to maximize vessel inclusion, and it provided the maximum likeliness to compute the PVS map. The output of this step is a quantitative map of vesselness (i.e., PVS map) in regions of interest (ROIs) and is taken to be the maximum across scales, as suggested by Frangi *et al.*[13] The range of voxel scale corresponded to the specific levels in scale space that are searched for tubular structure feature detectors. Thus, the PVS map included PVSs across a range of filter scales. Subsequently, PVS map $\mathcal{V}(s)$ in voxel s was standardized to avoid the influence of large outliers using robust scaling, in which values were scaled according to the interquartile range (abbreviated as IQR below) as follows:

$$\hat{\mathcal{V}}(s) = \frac{\mathcal{V}(s) - \mathcal{V}_{\min}}{\mathrm{IQR}(\mathcal{V})}. \qquad (1)$$

Then, the binary image of PVS mask $P(s)$ was obtained by thresholding $\hat{\mathcal{V}}(s)$:

$$P(s) = \begin{cases} 1 & \hat{\mathcal{V}}(s) \geq t \\ 0 & o.w. \end{cases}. \qquad (2)$$

In this study, the binary image of PVS mask $P(s)$ was segmented using a threshold value (t) of 2.3 and had 1 value when over the threshold, otherwise had 0

value. The threshold was optimized in a previous study that searched optimum values by maximizing their concordance with the expert visual reading.[16] The PVS mask was applied excluding the periventricular voxels and removed the incorrectly segmented PVSs at the lateral ventricle–WM boundary to avoid PVS mis-segmentation in the periventricular and superficial WM areas.

The WML mask was constructed from original FLAIR images using the Lesion Segmentation Toolbox implemented in Statistical Parametric Mapping 12 (https://www.fil.ion.ucl.ac.uk/spm/software/spm12/). This was then registered to the T1w image space by applying the FLAIR-to-T1w image transformation matrix obtained at the MRI data processing stage (eMethod 5); subsequently, the WML mask was subtracted from the PVS mask. The PVS masks of all study participants were further checked in a blinded manner by a neuroradiologist (K.K.) with 11 years of experience, and minimal manual correction was performed to include undetected PVSs and exclude incorrect ones.

eMethod 7

In calculating the ALPS index, the FA maps of all participants were registered linearly first and nonlinearly subsequently into the high-resolution FMRIB58_FA standard space image. One participant with the smallest degree of warping (i.e., with the smallest sum of squared differences) was selected for ROI placement. With the use of this participant's native color-coded FA map, spherical ROIs measuring 5 mm in diameter were placed in the projection and association areas at the level of the lateral ventricle bodies in the left and right hemispheres (Fig. 3). In the projection area, dominant fibers

run in the *z*-axis direction, perpendicular to both the *x*- and *y*-axes, whereas in the association area, dominant fibers run in the *y*-axis direction, perpendicular to both the *x*- and *z*-axes. The resulting ROIs were then registered to the same FA template. The position of ROIs was manually checked for each participant. Manual corrections were not performed because all ROIs were correctly placed.

Finally, we calculated the ALPS index as a ratio of the mean of the *x*-axis diffusivity in the projection area ($D_{xx,\mathrm{proj}}$) and *x*-axis diffusivity in the association area ($D_{xx,\mathrm{assoc}}$) to the mean of the *y*-axis diffusivity in the projection area ($D_{yy,\mathrm{proj}}$) and the *z*-axis diffusivity in the association area ($D_{zz,\mathrm{assoc}}$) as follows:

$$\text{ALPS index} = \frac{\text{Mean}\,(D_{xx,\mathrm{proj}}, D_{xx,\mathrm{assoc}})}{\text{Mean}\,(D_{yy,\mathrm{proj}}, D_{zz,\mathrm{assoc}})}. \qquad (3)$$

In addition, using the same ROIs, we extracted FA values in the projection and association areas. The average of the left and right of projection and association FA values were then used in the statistical analyses.

References

1. Andica C, Kamagata K, Hayashi T, et al. Scan–rescan and inter–vendor reproducibility of neurite orientation dispersion and density imaging metrics. Neuroradiology 2020;62:483–494.
2. Lee Y, Callaghan MF, Acosta–Cabronero J, Lutti A, Nagy Z. Establishing intra– and inter–vendor reproducibility of T_1 relaxation time measurements with 3T MRI. Magn Reson Med 2019;81:454–465.
3. Folstein MF, Folstein SE, McHugh PR. ″Mini–mental state″. A practical method for grading the cognitive state of patients for the clinician. J Psychiatr Res 1975;12:189–198.

4. Nasreddine ZS, Phillips NA, Bedirian V, et al. The Montreal Cognitive Assessment, MoCA: a brief screening tool for mild cognitive impairment. J Am Geriatr Soc 2005;53:695–699.
5. Pfeffer RI, Kurosaki TT, Harrah CH, Jr., Chance JM, Filos S. Measurement of functional activities in older adults in the community. J Gerontol 1982;37:323–329.
6. Hughes CP, Berg L, Danziger WL, Coben LA, Martin RL. A new clinical scale for the staging of dementia. Br J Psychiatry 1982;140:566–572.
7. Rosen WG, Mohs RC, Davis KL. A new rating scale for Alzheimer's disease. Am J Psychiatry 1984;141:1356–1364.
8. Battista P, Salvatore C, Castiglioni I. Optimizing Neuropsychological Assessments for Cognitive, Behavioral, and Functional Impairment Classification: A Machine Learning Study. Behav Neurol 2017;2017:1850909.
9. Corrigan JD, Hinkeldey NS. Relationships between parts A and B of the Trail Making Test. J Clin Psychol 1987;43:402–409.
10. Pantoni L, Inzitari D. Hachinski's ischemic score and the diagnosis of vascular dementia: a review. Ital J Neurol Sci 1993;14:539–546.
11. Andersson JL, Sotiropoulos SN. An integrated approach to correction for off-resonance effects and subject movement in diffusion MR imaging. Neuroimage 2016;125:1063–1078.
12. Basser PJ, Mattiello J, LeBihan D. Estimation of the effective self-diffusion tensor from the NMR spin echo. J Magn Reson B 1994;103:247–254.
13. Frangi AF, Niessen WJ, Vincken KL, Viergever MA. Multiscale vessel enhancement filtering. In: Medical Image Computing and Computer-Assisted Intervention — MICCAI'98 Lecture Notes in Computer Science [online]1998.
14. van der Walt S, Schönberger JL, Nunez-Iglesias J, et al. scikit-image: image processing in Python. PeerJ 2014;2:e453.
15. Donahue EK, Murdos A, Jakowec MW, et al. Global and Regional Changes in Perivascular Space in Idiopathic and Familial Parkinson's Disease. Mov Disord 2021;36:1126–1136.
16. Sepehrband F, Barisano G, Sheikh-Bahaei N, et al. Image processing approaches to enhance perivascular space visibility and quantification using MRI. Sci Rep 2019;9:12351.

ADNI Funding Resources

Data collection and sharing for ADNI were funded by the ADNI (National Institutes of Health grant no. U01 AG024904) and DOD ADNI (Department of Defense award number W81XWH-12-2-0012). The ADNI is funded by the National Institute on Aging, the National Institute of Biomedical Imaging and Bioengineering, and generous contributions from the following: AbbVie; Alzheimer's Association; Alzheimer's Drug Discovery Foundation; Araclon Biotech; BioClinica, Inc.; Biogen; Bristol-Myers Squibb Company; CereSpir, Inc.; Cogstate; Eisai Inc.; Elan Pharmaceuticals, Inc.; Eli Lilly and Company; EuroImmun; F. Hoffmann-La Roche Ltd. and its affiliated company Genentech, Inc.; Fujirebio; GE Healthcare; IXICO Ltd.; Janssen Alzheimer Immunotherapy Research & Development, LLC; Johnson & Johnson Pharmaceutical Research & Development LLC; Lumosity; Lundbeck; Merck & Co., Inc.; Meso Scale Diagnostics, LLC.; NeuroRx Research; Neurotrack Technologies; Novartis Pharmaceuticals Corporation; Pfizer Inc.; Piramal Imaging; Servier; Takeda Pharmaceutical Company; and Transition Therapeutics. The Canadian Institutes of Health Research provides funds to support ADNI clinic sites in Canada. Private sector contributions are facilitated by the Foundation for the National Institutes of Health (https://www.fnih.org). The grantee organization is the Northern California Institute for Research and Education, and the study is coordinated by the Alzheimer's Therapeutic Research Institute at the University of Southern California. ADNI data are disseminated by the Laboratory for Neuro Imaging at the University of Southern California.

Supplementary Figures

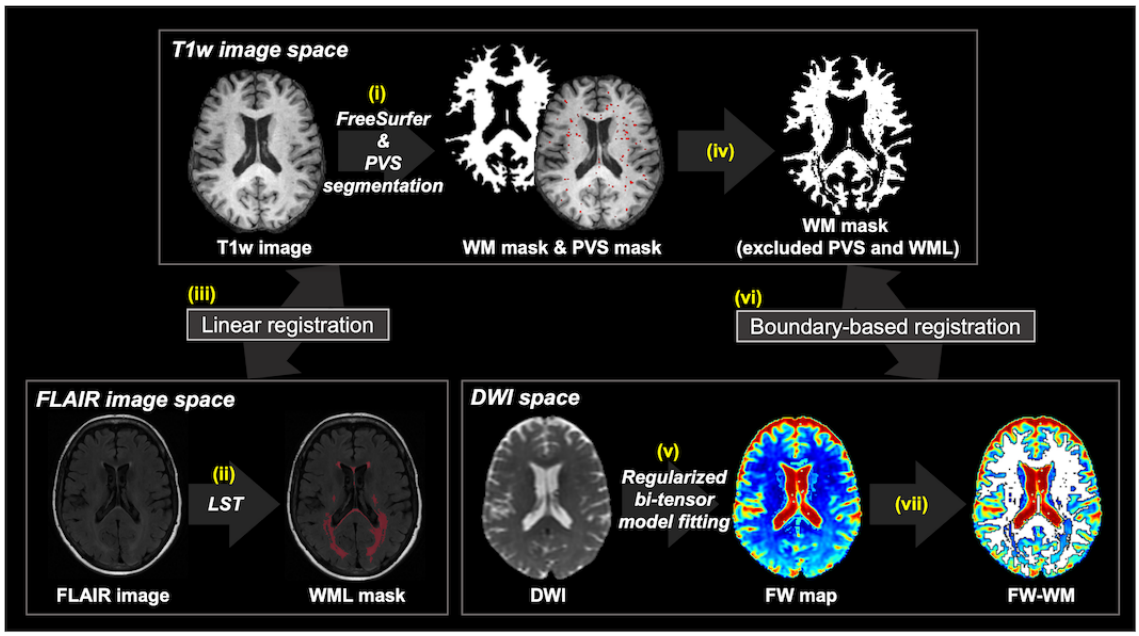

eFigure 1. Pipeline of the cerebral WM fractional volume of FW calculation. (i) The WM mask and PVS map were obtained using the FreeSurfer pipeline and PVS segmentation method described in the PVS segmentation subsection under Materials and methods. (ii) The WML mask was obtained using LST from the FLAIR image. (iii) The FLAIR image was linearly registered to the T1w image space using FLIRT, a part of FSL; the WML mask was also registered to the T1w image space. (iv) The WML mask and PVS map were subtracted from the WM mask to recreate the WM mask (excluding PVS and WML). (v) The maps of the fractional volume of FW were constructed by fitting DW images to a regularized bitensor model; the T1w and (vi) DW images were registered with boundary-based registration using epi_reg tool, a part of FSL, and the recreated WM mask was registered to the DW image space. (vii) Finally, the mean FW-WM was extracted using the recreated WM mask.

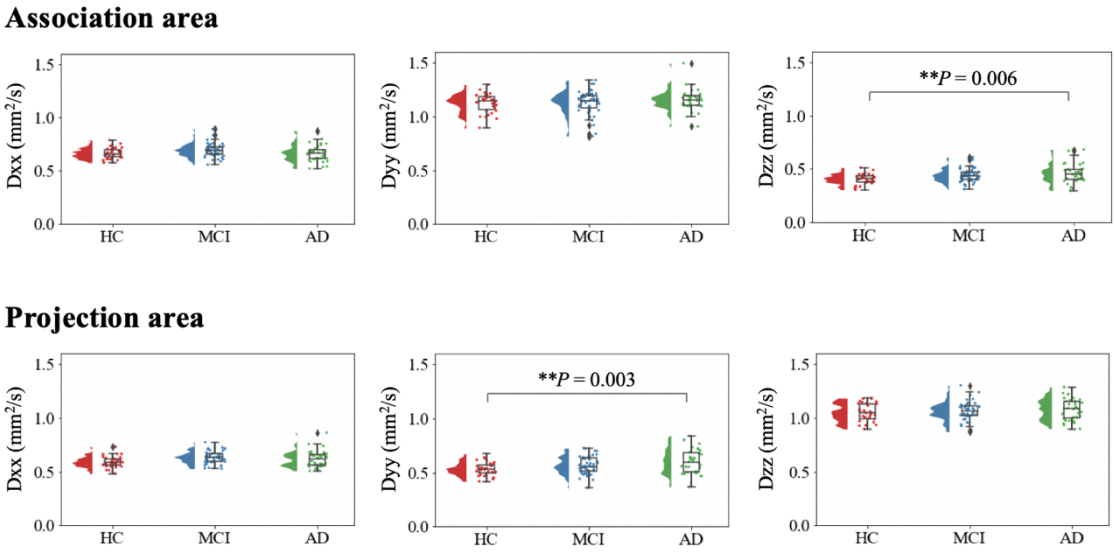

eFigure 2. Between-group differences in diffusivities in the association and projection areas. Violin and box plots of the x-,y-, and z-axis diffusivities in the association ($D_{xx,assoc}$, $D_{yy,assoc}$, and $D_{zz,assoc}$) and projection ($D_{xx,proj}$, $D_{yy,proj}$, and $D_{zz,proj}$) areas, respectively, among the healthy control (HC) participants, patients with MCI, and patients with Alzheimer's disease. *P* values correspond to the general linear model analysis. Statistical significance was set at $P < 0.05$.

eTable 1. Between-group differences in MRI measurements

	HC	MCI	AD	*P*-values			Cohen's *d*		
	Mean ± SD	Mean ± SD	Mean ± SD	HC vs. MCI	HC vs. AD	MCI vs. AD	HC vs. MCI	HC vs. AD	MCI vs. AD
Model 1									
PVSVF-ALL	0.0059 ± 0.0044	0.012 ± 0.0074	0.015 ± 0.0076	**0.006**	**<0.001**	0.081	0.99	1.48	0.41
PVSVF-WM	0.0040 ± 0.0035	0.0091 ± 0.0066	0.011 ± 0.0061	**0.018**	**<0.001**	0.223	0.91	1.34	0.27
PVSVF-BG	0.0011 ± 0.00062	0.0014 ± 0.00072	0.0019 ± 0.00084	0.063	**<0.001**	**0.050**	0.53	1.15	0.64
PVSVF-Hipp	0.0011 ± 0.00013	0.00019 ± 0.00017	0.00017 ± 0.00010	0.210	0.778	1.000	0.32	0.23	0.13
FW-WM	0.18 ± 0.018	0.18 ± 0.021	0.19 ± 0.021	0.724	**0.025**	0.255	0.27	0.73	0.43
Mean ALPS index	1.34 ± 0.11	1.33 ± 0.17	1.24 ± 0.21	1.000	**0.026**	0.137	0.07	0.63	0.52

Model 2			
PVSVF-ALL	**0.004**	**<0.001**	**<0.001**
PVSVF-WM	**0.007**	**<0.001**	**<0.001**
PVSVF-BG	0.563	**0.009**	0.149
PVSVF-Hipp	0.387	0.705	1.000
FW-WM	1.000	0.467	0.898
Mean ALPS index	0.133	0.057	1.000
Model 3			
Mean ALPS index	0.366	**0.040**	0.766
Model 4			
PVSVF-ALL	**0.003**	**<0.001**	**<0.001**
PVSVF-WM	**0.004**	**<0.001**	**<0.001**
PVSVF-BG	0.606	**0.020**	0.188
PVSVF-Hipp	0.318	0.499	1.000
FW-WM	1.000	0.491	0.881

Mean ALPS index	0.270	0.417	1.000
Model 5			
Mean ALPS index	0.593	0.278	1.000

P-values shown in this table were corrected via Bonferroni correction for between-group multiple comparisons. Bold values denote statistical significance at $P < 0.05$. Abbreviations: AD, Alzheimer's disease; HC, healthy controls; SD, standard deviation.

eTable 2. Partial correlation analysis between MRI measurements and clinical scores

	PVSVF-ALL		**PVSVF-WM**		**PVSVF-BG**		**PVSVF-Hipp**		**FW-WM**		**MeanALPS index**	
	r_s	*P*	r_s	*P*	r_s	*P*	r_s	*P*	r_s	*P*	r_s	*P*
Aβ42	−0.28	0.184	−0.25	0.447	0.09	0.783	0.10	0.836	−0.47	**0.021**	0.41	**0.019**
T-tau	0.17	0.411	−0.17	0.483	−0.04	0.819	0.03	0.913	−0.08	0.715	0.06	0.722
P-tau	0.19	0.391	0.18	0.483	−0.05	0.819	0.03	0.913	−0.08	0.715	0.08	0.681
FDG-PET	−0.15	0.442	−0.06	0.811	−0.14	0.617	−0.03	0.913	−0.28	0.157	0.54	**<0.001**
AV45-PET	0.17	0.391	0.16	0.483	0.08	0.783	−0.06	0.888	0.17	0.442	−0.08	0.681
MMSE	−0.27	0.156	−0.22	0.447	−0.14	0.617	0.09	0.836	−0.41	**0.021**	0.41	**0.013**
MOCA	−0.16	0.391	−0.11	0.640	−0.19	0.421	0.22	0.431	−0.14	0.458	0.23	0.209
FAQ	0.31	0.137	0.19	0.447	0.42	**0.026**	0.01	0.967	0.36	**0.044**	−0.38	**0.016**
CDR-SB	0.28	0.156	0.19	0.447	0.30	0.206	−0.03	0.913	0.30	0.101	−0.47	**0.003**
RAVLT-immediate	−0.11	0.497	−0.09	0.699	−0.05	0.819	0.10	0.836	−0.19	0.384	0.17	0.326

RAVLT-learni												
ng	−0.03	0.894	−0.03	0.822	−0.03	0.843	0.06	0.888	−0.16	0.442	0.19	0.297
RAVLT-forget												
ting	−0.06	0.698	−0.03	0.822	−0.13	0.617	−0.13	0.836	−0.14	0.458	0.20	0.274
RAVLT-%												
forgetting	0.02	0.896	0.05	0.811	−0.12	0.643	−0.28	0.302	0.04	0.831	0.12	0.536
ADAS-11	0.27	0.156	0.21	0.447	0.22	0.421	−0.10	0.836	0.31	0.101	−0.40	**0.013**
ADAS-13	0.19	0.338	0.15	0.483	0.18	0.442	−0.17	0.757	0.26	0.161	−0.33	**0.041**
ADAS-Q4	0.11	0.497	0.09	0.699	0.07	0.783	−0.27	0.302	0.07	0.715	−0.09	0.675
LDELTOTAL	−0.32	0.137	−0.22	0.447	−0.29	0.206	−0.12	0.836	0.00	0.980	0.05	0.722
TRABSCOR	0.35	0.121	0.29	0.447	0.26	0.206	−0.09	0.836	0.18	0.436	−0.18	0.309
Hipp volume	0.07	0.698	0.04	0.822	0.09	0.740	0.25	0.302	−0.09	0.715	0.30	0.103

The table shows false discovery rate (FDR)-adjusted *P*-values and partial Spearman's rank correlation coefficient (r_s). Bold values denote statistical significance at FDR-adjusted $P < 0.05$. Abbreviations: MOCA, Montreal Cognitive Assessment; T-tau, total tau; P-tau, phosphorylated tau